Long distance Bessel beam propagation through Kolmogorov turbulence

Article (Accepted Version)

Long Distance Bessel Beam Propagation Through Kolmogorov Turbulence

PHILIP BIRCH[1,*], INIABASI ITUEN[1], RUPERT YOUNG[1], AND CHRIS CHATWIN[1]

[1]Department of Engineering and Design, University of Sussex, Falmer, East Sussex,BN1 9QT,United Kingdom
[*]Corresponding author: p.m.birch@sussex.ac.uk

Compiled September 16, 2015

Free space optical communication has the potential to transmit information with both high speed and security. However, since it is unguided it suffers from losses due to atmospheric turbulence and diffraction. To overcome the diffraction limits the long distance propagation of Bessel beams is considered and compared against Gaussian beam properties. Bessel beams are shown to have a number of benefits over Gaussian beams when propagating through atmospheric turbulence.

OCIS codes: *(010.1300) Atmospheric propagation, (060.2605) Free-space optical communication, (050.1960) Diffraction theory*

http://dx.doi.org/10.1364/ao.XX.XXXXXX

1. INTRODUCTION

Free Space Optics (FSO) for data transmission has the potential to produce a very high capacity, secure and robust communication method[1–3]. Work has so far largely focused on the propagation of Gaussian beams. However, Gaussian beams suffer from diffraction, causing the spread of the beam's energy and so lowering the signal to noise ratio (SNR) at the receiver and increasing the bit error rate (BER). This paper investigates possible improvements to FSO by simulating the propagation of non-diffracting beams through unguided media. Gaussian beams suffer from diffraction and atmospheric turbulence effects. A non-diffracting self-healing Bessel beam could potentially mitigate these problems.

Bessel beams possess an intensity profile that is cylindrically symmetrical: a central core surrounded by a set of concentric rings. It has been shown that the central core of a Bessel beam is remarkably resistant to diffractive spreading compared to that of a Gaussian beam with a similar beam radius [4].

Bessel beams can be decomposed into an infinite set of plane wave-fronts at different azimuths, but at a fixed inclination towards the direction of travel. When propagating, these wave-fronts travel inwardly adding to the energy of the central core [5, 6]. This inward propagation helps the on-axis intensity to remain constant as it propagates. Another effect of the inward diffraction is an attribute called self- healing: the beam is capable of recovering back its profile after being partially scattered by an obstruction. These properties make Bessel beams very promising for various applications such as in terrestrial and satellite communications, microscopy [7, 8] and the optical manipulation of matter [9, 10].

One of the drawbacks of a Bessel beam is that to create a true non-diffracting beam, the amplitude field of the beam must have infinite radius and therefore power. Physically produced beams are therefore an approximation in which the aperture function of the optical system actually limits the extent over which a Bessel beam will be non-diffracting. In this paper, we analyse the maximum range over which a Bessel beam could be realistically produced. Other authors [4] have shown that the Bessel range is approximately equal to the Gaussian half intensity range multiplied by the number of rings in the Bessel beam. At first it appears that the Bessel beam offers significant advantages, but we will show that this advantage is curtailed by the increase in size of the optics required to produce the beam.

In this paper we simulate the propagation of both Gaussian and Bessel beams from ground level, through atmospheric turbulence. Previously, Nelson *et al.* [11] investigated the propagation of these beams within a short ground-to-ground range of 6.4km, with constant strength of turbulence. They showed how the ring structure is disrupted by the atmosphere and that there is an increasing on axis intensity loss with an increasing number of rings. In this paper we investigate the more difficult long distance propagation from ground to space, with the C_n^2 larger in the lower atmosphere but gradually weakening with altitude based on a modified Hufnagel-Valley model[12, 13] over a considerably larger distance.

In sections 2 and 3 we will compare the basic properties of Gaussian beams and Bessel beams. Since both beams, strictly speaking, have infinite support but in practice an aperture function that curtails this, we define a method of comparing the two beams. Section 4 will discuss how to select a Bessel beam for the maximum propagation distance possible with a given aperture; section 5 will discuss how such a beam could be physically produced; section 6 will discuss the propagation of the beams

through turbulence; and section 7 presents the discussion.

2. GAUSSIAN BEAM PROPERTIES

Lasers with Gaussian beam profiles are extremely common and their propagation through vacuum and atmospheric turbulence is well understood [14]. The power of the beam through an aperture of radius r is:

$$P = P_0\left(1 - \exp(-2r^2/w(z)^2)\right) \tag{1}$$

where $P_0 = \pi/2 I_0 w_0^2$, w_0 is the initial beam width and I_0 is the peak intensity. An aperture of radius $1.5174w_0$ at $z = 0$ is therefore required such that 99% of the beam power is transmitted. Assuming that the receiver telescope has a radius equal to $1.5174w_0$ the width of the initial beam's waist in which half of the beams power has been lost when it reaches the receiver is

$$w(z) = 2.5775 w_0 \tag{2}$$

and the distance travelled over which half the power is lost is then:

$$z_{dp} = 1.2560\frac{\pi w_0^2}{\lambda} \tag{3}$$

The waist radius of the aperture to ensure only half the power is lost is:

$$w_0 = 1.5174\sqrt{\frac{z\lambda}{1.2560\pi}} \tag{4}$$

Table 1 shows various beam widths required for Gaussian propagation. For objects up to low Earth orbit, small telescopes perform reasonably well. However, communication with GPS and GSO require large diameter telescopes comparable to a radio wave dish with a much larger value for λ. Ideally, a non-diffracting beam would be better in these scenarios.

3. BESSEL BEAM PROPERTIES

An ideal Bessel beam of the n^{th} order can be represented by [6]

$$E(r,\phi,z) = A_0 \exp(ik_z z)\, J_n(k_r r) \exp(\pm in\phi) \tag{5}$$

where k_r is the radial wave-vector, k_z is the longitudinal wave-vector, r is the radial coordinate, i.e., $r^2 = x^2 + y^2$, and:

$$k = \sqrt{k_z^2 + k_r^2} = \frac{2\pi}{\lambda} \tag{6}$$

For $n = 0$, which is normally the case for Bessel beams and will be used in the rest of this paper, equation 5 can be decomposed as follows:

$$E(r,\phi,z) = A_0 \exp(ik_z z) \int_0^{2\pi} \exp\left[ik_r\left(x\cos\phi + y\sin\phi\right)\right]\frac{d\phi}{2\pi} \tag{7}$$

This shows how the Bessel beam can be considered as an infinite set of plane waves, each one at angle θ to the direction of travel. The normals of each plane therefore produce a cone shape. Following [6], the angle of the cone defined by the Bessel beam's wave-front is:

$$\theta = \arctan\left(\frac{k_r}{k_z}\right) \tag{8}$$

and the beam radius is defined as the central core spot radius, i.e., the location of the first root of $J_0(k_r r)$ is:

$$b_w = \frac{2.405}{k_r} \tag{9}$$

Equation 5 is not physically realisable since it is of infinite extent. In practice there will be some aperture function, $B(r,\phi)$, which limits the distance over which the beam will be non-diffracting. Here we assume $B(r,\phi)$ is a circular aperture with radius B_w. The maximum propagation distance the Bessel beam can propagate is a simple geometric relationship [5]:

$$z_{max} = \frac{B_w k}{k_r} = \frac{B_w}{\tan\theta} \tag{10}$$

Thus, to produce a Bessel beam that propagates a long distance, either B_w is large, making the telescope large, or k_r is small.

The power contained in the Bessel beam up to radius b is found by integrating equation 5:

$$P = A_0^2\int_0^{2\pi}\int_0^b J_0^2(rk_r)\,r\,dr\,d\phi = A_0^2 b^2\pi\left(J_0(k_r b)^2 + J_1(k_r b)^2\right) \tag{11}$$

When we set $b = B_w$ and $k_r = 2.4048/B_w$ this is the power from the central peak up to the first zero in equation 5:

$$P_{B_w} = A_0^2 B_w^2 \pi J_1(2.4048) = 0.8467 A_0^2 B_w^2 \tag{12}$$

We assume that a Gaussian beam is generated with a w_0 such that 99% of its power passes through an aperture of radius B_w and a Bessel beam is generated with 100% of the laser power within B_w. Then equating Equation 12 with Equation 1 shows that the peak intensity of the Bessel beam is 1.1764 times greater than the peak intensity of the Gaussian.

Since the Bessel beam is non-diffracting up to a distance z_{max}, a first thought might be that the power of the Bessel beam contained within the initial aperture function should remain high up to and beyond z_{max}. However, this is not the case due to the aperture function. Figure 1 shows a representation of equation 7 but for a single value of $\delta\phi$. Q is the cylinder extruded by the plane wave at angle θ after its interaction with the aperture. W is the cylinder extruded from the aperture function itself. For there to be no power loss Q must remain within W but it is clear from the diagram that there is only a limited area, A = Q ∩ W, in which the overlap occurs and this is a function of z and θ.

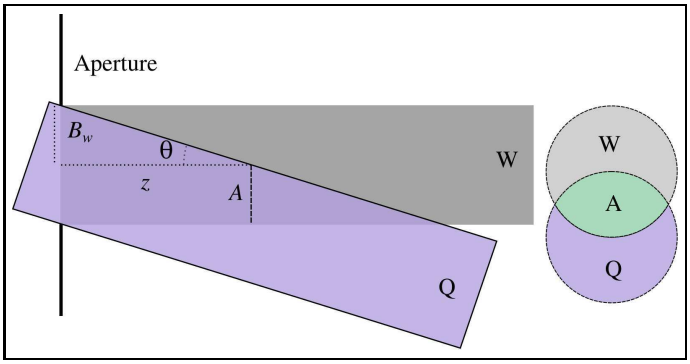

Fig. 1. Bessel beam decomposed into a plane wave Q which diverges from the aperture function W over distance z.

The energy contained with the single plane wave-front at angle $\delta\phi$ is then the integral of the wave-front over A. Integrating

over all ϕ then gives the power contained with cylinder W.

$$P(z) = \left| \iint_A \int_0^{2\pi} \exp\left[ik_r\left(x\cos\phi + y\sin\phi\right)\right] \frac{d\phi}{2\pi} dxdy \right|^2 \quad (13)$$

$$P(z) = \left| \iint_A J_0(k_r r) dxdy \right|^2 \quad (14)$$

This simple model ignores diffraction effects from the aperture but simulations suggest that it is a reasonable model. Figure 2 shows the total beam power within the original aperture versus propagation distance calculated with Equation 14 and by computer simulated Fresnel diffraction [15] for three different values of k_r.

To find the point at which half the power was lost stimulations were performed. For a range of apertures from $0.01m$ to $1m$ the distance over which half the beam power was lost was calculated by propagating the Bessel beam using a Fresnel propagation code and using Equation 14. The half power distance appears to be at z_{max}. However, when the value of k_r is small such that the first root of the Bessel function equals the radius of the aperture function, the distance appears to be a constant in terms of z_{max} at a value of $(1.1803532 \pm 0.0000067)z_{max}$.

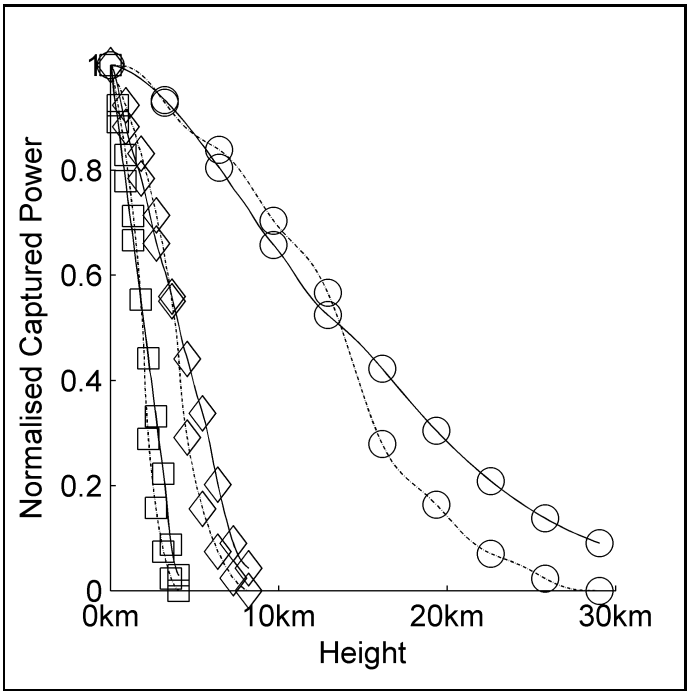

Fig. 2. Power contained within the original aperture versus distance of propagation for a Bessel beam. The geometric power model (dashed line) and Fresnel diffraction model (solid line) are compared for different values of k_r. Legend: $\square$ $k_r = 0.0039m^{-1}$,$\Diamond$ $k_r = 0.0079m^{-1}$, $\bigcirc$ $k_r = 0.0278m^{-1}$

The additional distance factor can be understood since for small values of k_r the area A is always a subset of the larger central lobe of the Bessel function. When k_r is larger the area A samples the smaller outer oscillations of the Bessel function, thus reducing the total power within the beam.

4. SELECTION OF B_W

It can be seen in Table 1 that using a large diameter telescope will enable the long distance transmission of light with a Gaussian beam profile without much loss due to diffraction. Clearly though, the large diameter of the telescope has cost implications as well as additional weight, size and inconvenience, especially for space based applications.

From Equation 10, if we ensure the amplitude of the Bessel beam is zero at the edge of the aperture function, we find an equation for the minimum radius of the beam:

$$B_w^{min} = \sqrt{\frac{2.405 z_{max}}{k}} \quad (15)$$

However, as noted above when k_r is small, the half power distance is actually at $1.18z_{max}$ so Equation 15 is modified to be:

$$B_w^{min} = \sqrt{\frac{2.405 z_{max}}{1.18k}} \quad (16)$$

Examples for different transmission distances are shown in Table 1.

Calculation of the on-axis intensity can be performed by direct integration of the Fresnel diffraction equation. The on-axis intensity for a radially symmetric function $A(r)$ is given by [16]:

$$I(0,z) = \left(\frac{k}{z}\right)^2 \left| \int_0^{B_w} rA(r) \exp\left(\frac{ik\rho^2}{2z}\right) dr \right|^2 \quad (17)$$

The on axis intensities for various values of k_r are shown in Figure 3. For this $B_w = 44mm$ and so for the Bessel beam root to be at the edge of the aperture $k_r = 54m^{-1}$. It can be seen that the maximum propagation length can be increased further than this but at the cost of increased ringing effects from the edge of the aperture.

5. BESSEL BEAM PRODUCTION

A Bessel beam can be produced from the Hankel transform of a radially symmetric delta functional $\delta(r - k_r)$, which is a infinitely thin ring structure [5]. However, this is extremely light inefficient. The two most common methods for the production of Bessel beams in the lab are based on either an axicon [17] or by the direct modulation of phase [18] or amplitude [19] by a computer generated hologram (CGH) often implemented using a spatial light modulator (SLM) [18, 20]. We note that the delta function and phase wedge of the axicon/CGH are both Hankel transform pairs. We also note that is also possible to directly encode the Bessel beam function in Equation 5 directly onto a hologram that is capable of producing negative amplitudes, i.e., a π shift in phase.

An alternative promising method of production includes the direct generation from customised lasers [21, 22]. We also note that since the Bessel beam in this paper has no rings with negative amplitude components, it would possible to convert a Gaussian laser beam profile with a suitable intensity mask.

A number of authors [19, 20, 23, 24] have implemented phase only holograms that are intrinsically light efficient. These systems encode the CGH or SLM with the phase profile:

$$T(\rho,\theta) = \exp(in\theta)\exp(-i2\pi r/k_r) \quad (18)$$

which for $n = 0$ is the same profile as that produced by an axicon.

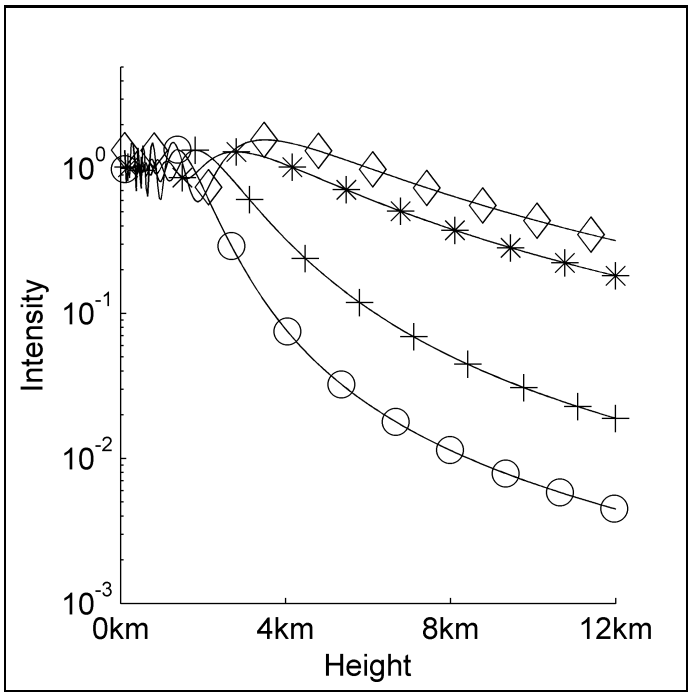

Fig. 3. On-axis intensity of the Bessel beam versus distance for $B_w = 0.044m$ for different values of k_r. Legend: $\circ$ $k_r = 197m^{-1}$;$+$ $k_r = 125m^{-1}$;$*$ $k_r = 55m^{-1}$;$\diamond$ $k_r = 45m^{-1}$. The radial frequencies are such that the aperture equals: the third root; the second root; the first root; and 83% of the first root of the Bessel function respectively.

For low values of k_r, as discussed in this paper, this would not produce a satisfactory Bessel beam since it maybe grossly under sampled. For example, when using a binary SLM and $k_r/B_w < 2.405$ the phase of the modulation signal will be $+\pi$ for the whole SLM.

The axicon method has been shown to have greater light efficiency, at nearly 100%, when compared to CGH methods[25] which is important for this application. However, production would be challenging. To produce a Bessel beam using an axicon, the opening angle of the axicon, γ, is related to θ via:

$$\theta = (n_1/n_2 - 1)\gamma \tag{19}$$

so

$$z_{max} \approx \frac{B_w}{\theta} = \frac{B_w}{\gamma\,(n1/n2 - 1)} \tag{20}$$

where n_1 is the refractive index of the axicon material and n_2 is that of the surrounding medium where the light exits the axicon (1 for air).

For $B_w = 44mm$, $z_{max} = 12km$, $n_1 = 1.5$ and $n_2 = 1.0$, the angle of the axicon would only be 1.5 arc-seconds making the centre $0.32\mu m$ thick which is not easy to build. If axicon was immersed in an index matching material such that $n1 - n2 = 0.001$ the opening angle of the axicon becomes a more physically realisable $\gamma = 0.3^\circ$ for $B_w = 44mm$ and $z_{max} = 12km$. For the most extreme case, the GSO in Table 1, with $B_w = 2.41m$ and $z_{max} = 35,786km$, $\gamma = 0.34$ arc-minutes. The production of this beam would still be possible with the correct phase angle by using the $\gamma = 0.3^\circ$ axicon and a $54.4\times$ magnification telescope.

6. ATMOSPHERIC SIMULATION

To simulate propagation through the atmosphere Fresnel diffraction was employed. The simulation assumes the transmitter is at ground level and then propagates vertically a distance $22km$ through the atmosphere. After $22km$ the turbulence effects are assumed to be negligible and so the beam is propagated a further $78km$ in a vacuum. The wavelength, $\lambda = 500nm$ and the inner and outer atmospheric scales were $l_0 = 0.01m$ and $L_0 = 100m$. The total data array size was 1024×1024 and represented an array of width $40 \times B_w$. Each propagation distance was $220m$ and the simulation was repeated 100 times to get a mean measurement.

The beam aperture, B_w, was varied from $0.044m$ to $3.23m$ as in Table 1. The value of k_r is set such that the Bessel beam's first zero or root is equal to the aperture width. This was compared against a Gaussian beam with aperture equally to B_w and w_0 such that 99% of the power could pass through. Both beams pass through identical sets of randomly generated atmospheric phase screens.

We use beam power to compare the two beams since we assume that both beams would be generated from the same laser system. Using other metrics such as the full width half maximum (FWHM) can be misleading since the two beams have a different intensity cross sectional shape. The central lobe of the Bessel beam is slightly narrower than a Gaussian beam of the same peak intensity giving a different total beam power for the same beam FWHM.

To simulate atmospheric turbulence the Andrews [26] variant of the Hufnagel-Valley C_n^2 model was used in which we assume the propagation starts from sea-level and C_n^2 is the refractive index structure parameter:

$$C_n^2(h) = 6.5\Big[3.593\times10^{-3}\left(\frac{h}{10^5}\right)^{10} \exp(-h/1000) + 2.7\times10^{-16}\exp(-h/15000)\Big] \tag{21}$$

where h is the height above sea-level. This provides an approximate model for the refractive index structure parameter which ranges from $C_n^2(0) = 1.755\times10^{-15}$ to $C_n^2(22km) = 1.731\times10^{-18}$ and gives a Fried parameter of $0.038m$ through all the modelled layers.

The phase screens are generated every $220m$ using Equation 21 and the inverse Fourier transform method is employed with additional sub-harmonics as described in [27, 28] which uses the modified von Kármán power spectrum:

$$\Phi(\kappa) = 0.033C_n^2\frac{\exp\left(-\kappa^2/\kappa_m^2\right)}{\left(\kappa^2+\kappa_0^2\right)^{11/6}} \tag{22}$$

where κ is the angular spatial frequency, $\kappa_m = 5.92/l_0$ and $\kappa_0 = 2\pi/L_0$. No additional inner scale effects where modelled.

The following metrics were measured: the peak intensity; the peak to side-lobe ratio; the peak position error; the RMS intensity error from the beam at $z = 0$; and the total power captured by a receiver of the same aperture as the transmitter.

The propagation is halted if any power is detected at the edge of an array. With our choice of parameters these cases are due to the diffraction of the beam overfilling the array rather than beam wander. In these cases, the actual captured beam power will then be low and so the experiment can be safely halted. This happens after approximately $5km$ for the

$B_w = 44mm$ case and $16km$ for the $B_w = 77mm$ case. The larger beam width are successfully simulated through the $22km$ of atmosphere. Figure 4 shows the intensity cross sections versus propagation distances for the Bessel and Gaussian beams.

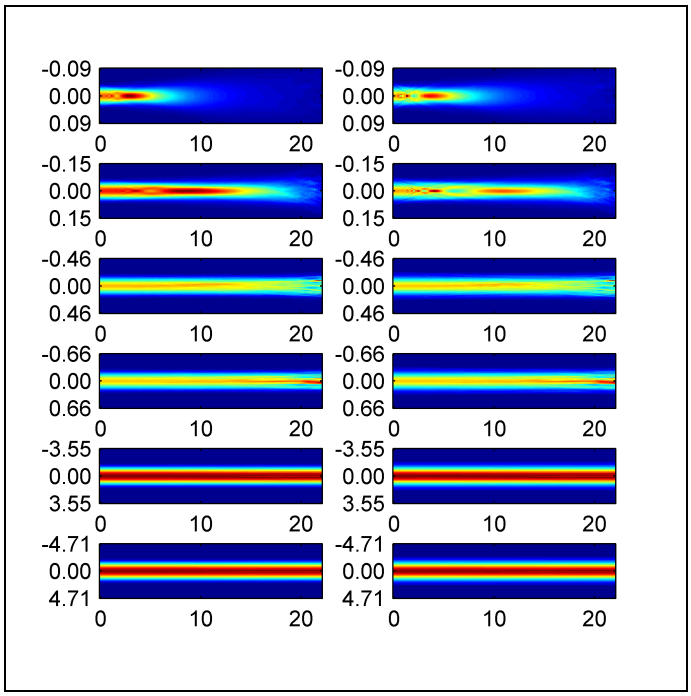

Fig. 4. The intensity cross-sections versus distance with a false colour map. The left hand images are the Bessel beams and the right hand images are the Gaussian beams. The vertical axis are the beams' radial coordinates in metres and the horizontal axis are the propagation heights in kilometres. The initial beam widths are taken from Table 1

7. DISCUSSION

To facilitate a good a FSO communication system, the transmission beam needs to have a high peak intensity with a high peak power and it must not wander due to turbulence away from the receiver. In addition, it is beneficial for the transmitter optics to be as small as possible. We will now discuss if these criteria can be achieved using Bessel beams. Table 1 shows that the aperture radius to transmit to the half power loss distance is smaller for Bessel beams than for Gaussian beams. This is possible since we have shown that to get the maximum propagation distance the Bessel beams' radial frequency, k_r, should be set such that the aperture radius equals the first root of the Bessel function.

Figure 5 shows the amount of power captured by a receiver of the same diameter as the transmitter. Both the Gaussian and Bessel beams start with the same amount of power and so Figure 5 shows that the Bessel beam actually slightly out performs the Gaussian beam in this metric.

To test the propagation code, Figure 6 shows several graphs: the theoretical power captured by an aperture of $77mm$ from Equation 1; the Fresnel diffraction result with and without any $77mm$ aperture at ground level (i.e. the telescope is assumed to fill the entire numeric array), which is shown for both Bessel and Gaussian beams. The parameters used were for the High Altitude Aircraft in Table 1. This shows several interesting

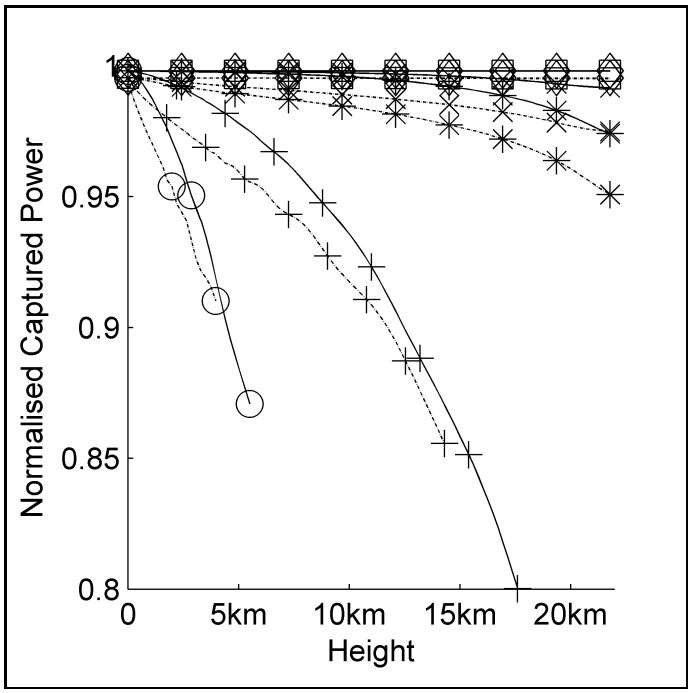

Fig. 5. The amount of power captured by a receiver of the same radius as B_w versus height. Solid lines are the Bessel beams, dashed lines are Gaussian beams. The radii of the apertures for each symbol are shown in Table 1

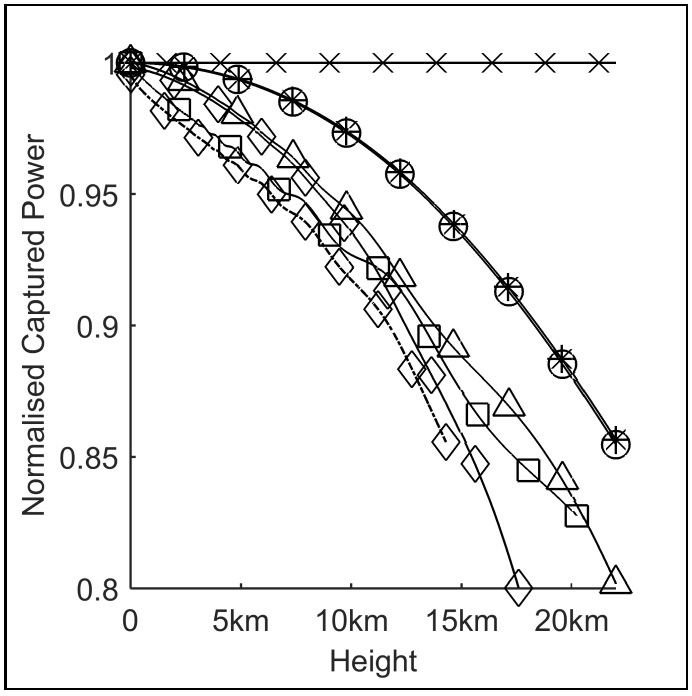

Fig. 6. The power captured by a receiver of the same radius as $B_w = 77mm$ versus height *in vacuo*. × Bessel beam with no ground level aperture; ∗ theoretical power from equation 1; ○ Fresnel simulation code for the Gaussian beam with no ground level aperture; △ Bessel beam with an aperture; □ Gaussian beam with an aperture; ◇ shows the power with the simulated turbulence, the solid line is the Bessel beam and the dashed line is the Gaussian beam.

Table 1. Useful Propagation Targets and Distances. [a] is the beam width of the transmitter and receiver required for only half the power of a Gaussian beam to be lost. [b] is the Bessel beam aperture radius, B_w, given by Equation 16

Label	Target	Height above sea level	Beam width[a]	B_w[b]
○	A320 Aircraft ceiling	$12km$	$59mm$	$44mm$
+	High Altitude Aircraft	$27km$	$89mm$	$77mm$
∗	International Space Station (ISS)	$340km$	$315mm$	$235mm$
×	Low Earth Orbit (LEO) Satellite	$700km$	$452mm$	$337mm$
□	Global Position System (GPS) Satellite	$20,350km$	$2.44m$	$1.82m$
◇	Geostationary orbit (GSO)	$35,786km$	$3.23m$	$2.41m$

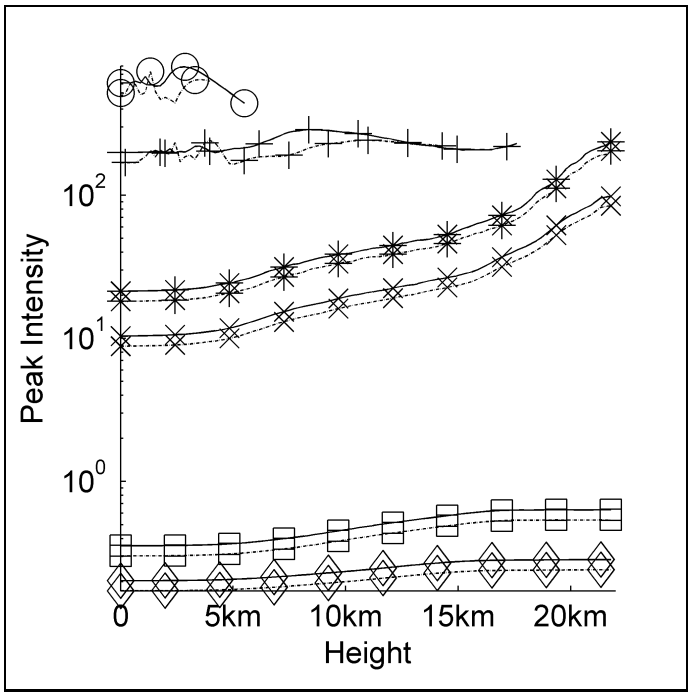

Fig. 7. The peak intensity of the beam versus height. Solid lines are the Bessel beams, dashed lines are Gaussian beams. The radii of the apertures for each symbol are shown in Table 1

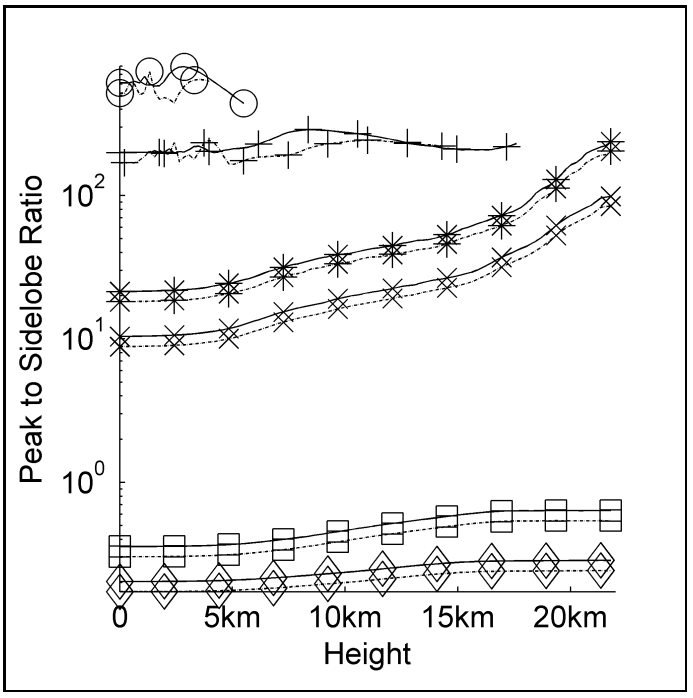

Fig. 8. The peak intensity to side lobe ratio of the beams versus height. Solid lines are the Bessel beams, dashed lines are Gaussian beams. The radii of the apertures for each symbol are shown in Table 1

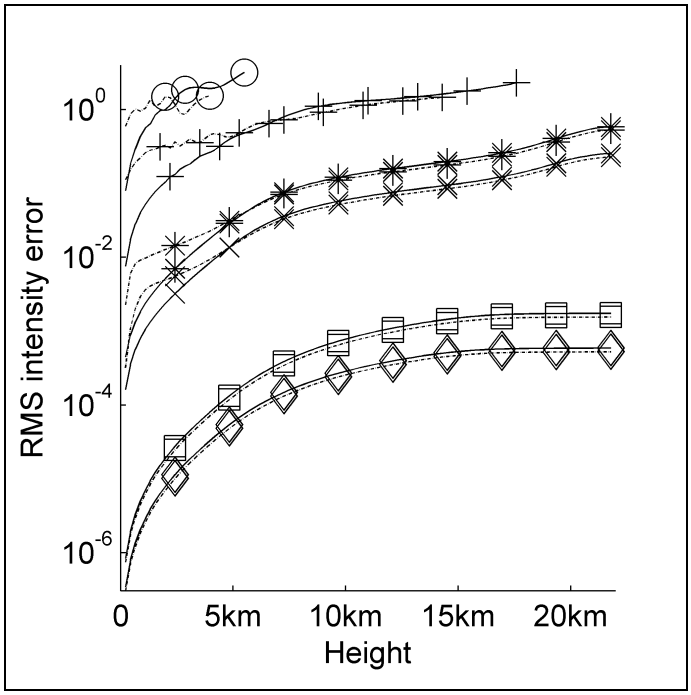

Fig. 9. The RMS intensity error versus height. The error is defined as the propagated intensity minus the intensity of the beam at sea-level. Solid lines are the Bessel beams, dashed lines are Gaussian beams. The radii of the apertures for each symbol are shown in Table 1

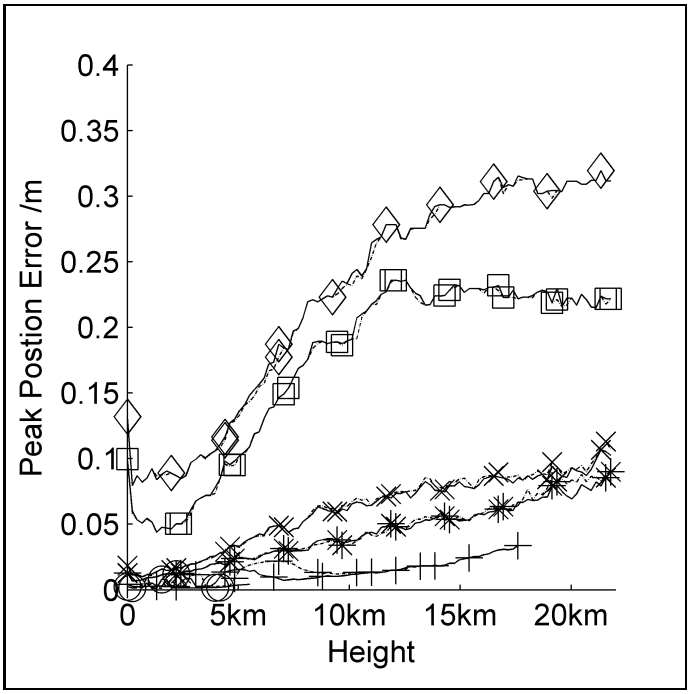

Fig. 11. The peak position error versus height. Solid lines are the Bessel beams, dashed lines are Gaussian beams. The radii of the apertures for each symbol are shown in Table 1

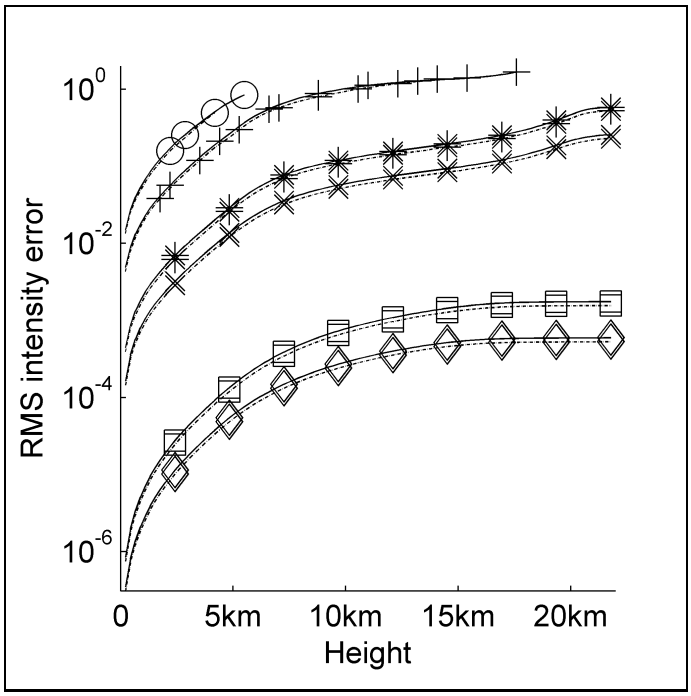

Fig. 10. The RMS intensity error versus height. The error is defined as the propagated intensity minus the intensity of the unaberrated beam that has travelled the same distance. Solid lines are the Bessel beams, dashed lines are Gaussian beams. The radii of the apertures for each symbol are shown in Table 1

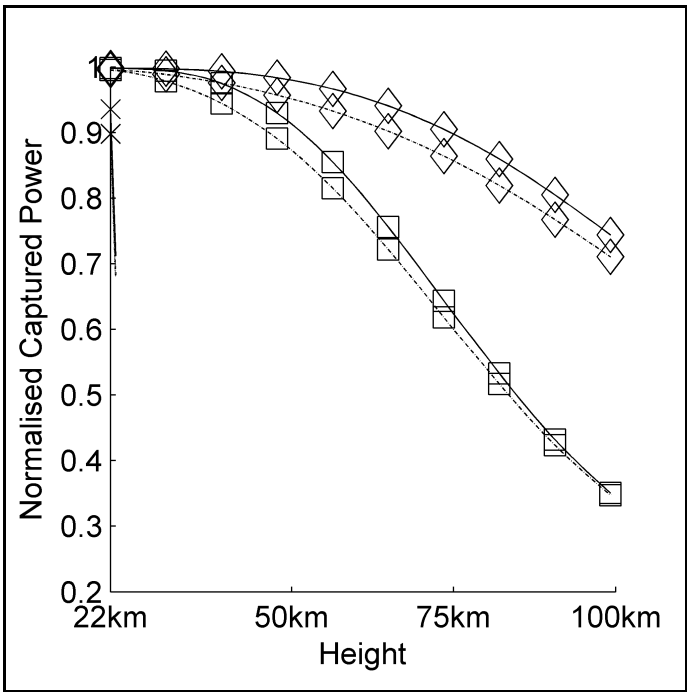

Fig. 12. The amount of power captured by a receiver of the same radius as B_w versus height for distances greater than $22km$. The propagation is assumed to be *in vacuo*. Solid lines are the Bessel beams, dashed lines are Gaussian beams. The radii of the apertures for each symbol are shown in Table 1

points. Firstly, the Gaussian propagation with no starting aperture has a very close result to the Fresnel propagation result giving us confidence in the simulation code. Secondly, the aperture introduced at ground level from the physical edge of the simulated telescope introduces significant ringing and power loss for both the Bessel and Gaussian beams. Without the aperture, the Bessel beam looses no power over the propagation distance. Thus, with the ground level aperture in place the Bessel beam outperforms the equivalent Gaussian beam. The effects of the atmosphere can also been seen. The $\diamond$ markers indicate the captured power with the turbulence simulation added. With the turbulence simulation the power captured drops to the 80% point on the graph earlier than the *in vacuo* simulation.

Figures 7 to 10 are intensity measurements. Since the Bessel and Gaussian beams are set to have unity power, the peak intensity of the Bessel beam will be slightly higher then the equivalent Gaussian beam, and the peak intensity drops as the aperture is increased. Figure 7 shows the peak intensity. From Equation 12 the Bessel beam has a slightly higher peak intensity than the Gaussian beam. This can also be seen in Figure 7. The graph also shows that this peak intensity advantage is maintained over distance and through atmospheric turbulence. A similar result is shown in Figure 8 which graphs the peak intensity to side-lobe ratio of the beams. A large value indicates that power is concentrated in the centre region and not spread out over the field. The two graphs are very similar since most of the side-lobe power is captured by the receiver. Some of the ringing from the aperture edge seen in Figure 3 is evident but this is reduced since the peak intensity can be anywhere within the beam aperture and not just on the optical axis. We note that there is no ringing when we consider the integrated total power as in Figure 5.

Figure 9 shows the RMS error in the beam intensity when compared to the original beams at $z = 0$. Here, a lower value is better. The Gaussian beam slightly out performs the Bessel beam in this case. This is possibly because the Gaussian beam is more spread out than the Bessel beam, so atmospheric induced phase errors have less effect. Figure 10 shows a similar result except the propagated beam is compared to an identical propagated beam that has travelled the same distance but experiences no atmospheric turbulence. Again it can be seen that the Gaussian beam has a marginal advantage over the Bessel beam. We conclude that the Bessel beam is slightly more effected by turbulence than the Gaussian.

Figure 11 shows the error due to beam wander by measuring the position of peak intensity. Both the Bessel and the Gaussian beam have almost identical results. The self-healing aspect of the Bessel beam can be seen to have little or no effect when the beam is subjected to phase errors.

Figure 12 shows the captured power after the beam has left the atmosphere. Above $22km$ the propagation is assumed to be *in vacuo*. It can be seen that both of the beams continue propagating.

It can be seen from the Figures 5 to 12 that the Bessel beam has an advantage over a Gaussian beams of the same power. The aperture radius is slightly smaller and the peak intensity and power captured is better for the Bessel beam. The beam wander appears to be identical for both beams.

To maintain this advantage though, the Bessel beam needs to produced from a laser with very high efficiency. It also needs to be produced with no side-lobes to make our comparisons accurate. Gaussian beams here have the advantage since many lasers produce beams with a near Gaussian profile inherently. As discussed in section 5 the axicon method has a high efficiency and the production of one for such a long range would be challenging but not impossible.

These results are in line with other authors simulations such as Nelson *et al.* [11] who showed that the turbulence disrupts the ring structure of the Bessel beams and that the best power transmission is when that Bessel beam has no rings at all as in our case. In their paper they describe this case as a truncated Gaussian beam. We have, however, shown that this is not the case and the ring-less Bessel beam does actually perform better than a Gaussian beam.

In conclusion, we have analysed various properties of both Bessel and Gaussian beams in this paper with respect to long distance propagation. We have shown that when considering long distance propagation for FSO communications Bessel beams have a number of advantages over Gaussian beam profiles in terms of power delivery. This is, however, provided that the Bessel beam can be produced efficiently. In addition to this we have shown that to maximise the distance for a given aperture that the beam can propagate, the radial frequency of the beam should be such that the aperture equals the first root of the Bessel function.

We have used the power through an aperture to compare the two types of beam since we are assuming that a laser of fixed power is used to generate both beams. The practical difficulties of the Bessel beam's production may mean that in many cases it would better to use a Gaussian beam and to overcome the loss of power at the receiver by simply using a more powerful laser to generate the beam.

REFERENCES

1. X. Zhu and J. M. Kahn, "Free-space optical communication through atmospheric turbulence channels," IEEE Transactions on Communications **50**, 1293–1300 (2002).
2. J. C. Juarez, A. Dwivedi, A. R. Hammons, S. D. Jones, V. Weerackody, and R. A. Nichols, "Free-Space Optical Communications for Next-generation Military Networks," Communications Magazine, IEEE **44**, 46–51 (2006).
3. S. M. Navidpour, M. Uysal, and M. Kavehrad, "BER Performance of Free-Space Optical Transmission with Spatial Diversity," Wireless Communications, IEEE Transactions on **6**, 2813–2819 (2007).
4. J. Durnin, J. H. Eberly, and J. J. Miceli, "Comparison of Bessel and Gaussian beams," Optics Letters **13**, 79–80 (1988).
5. J. Durnin and J. J. Miceli, "Diffraction-free beams," Physical Review Letters **58**, 1499–1501 (1987).
6. D. McGloin and K. Dholakia, "Bessel beams: diffraction in a new light," Contemporary Physics (2005).
7. L. Gao, L. Shao, B.-C. Chen, and E. Betzig, "3D live fluorescence imaging of cellular dynamics using Bessel beam plane illumination microscopy," Nature Protocols **9**, 1083–1101 (2014).
8. T. A. Planchon, L. Gao, D. E. Milkie, M. W. Davidson, J. A. Galbraith, C. G. Galbraith, and E. Betzig, "Rapid three-dimensional isotropic imaging of living cells using Bessel beam plane illumination," Nature Methods **8**, 417–423 (2011).
9. D. McGloin, V. Garcés-Chávez, and K. Dholakia, "Interfering Bessel beams for optical micromanipulation," Optics Letters **28**, 657–659 (2003).
10. J. Arlt, V. Garcés-Chávez, W. Sibbett, and K. Dholakia, "Optical micromanipulation using a Bessel light beam," Optics Communications **197**, 239–245 (2001).
11. W. Nelson, J. P. Palastro, C. C. Davis, and P. Sprangle, "Propagation of Bessel and Airy beams through atmospheric turbulence," JOSA A **31**, 603–609 (2014).
12. R. E. Hufnagel, "Propagation through atmospheric turbulence," in "The Infrared Handbook," (Washington, DC., 1974).

13. G. C. Valley, "Isoplanatic degradation of tilt correction and short-term imaging systems." Applied Optics **19**, 574–577 (1980).
14. B. E. A. Saleh and M. C. Teich, *Fundamentals of Photonics (Wiley Series in Pure and Applied Optics)* (John Wiley & Sons, 1991), 1st ed.
15. J. B. Breckinridge and D. G. Voelz, *Computational Fourier Optics*, A MATLAB Tutorial (SPIE-International Society for Optical Engineering, 2011).
16. Z. Jiang, Q. Lu, and Z. Liu, "Propagation of apertured Bessel beams," Applied Optics (1995).
17. V. Jarutis, R. Paškauskas, and A. Stabinis, "Focusing of Laguerre–Gaussian beams by axicon," Optics Communications **184**, 105–112 (2000).
18. N. Chattrapiban, E. A. Rogers, D. Cofield, W. T. Hill, III, and R. Roy, "Generation of nondiffracting Bessel beams by use of a spatial light modulator," Optics Letters **28**, 2183–2185 (2003).
19. A. Vasara, J. Turunen, and A. T. Friberg, "Realization of general nondiffracting beams with computer-generated holograms," JOSA A **6**, 1748–1754 (1989).
20. J. A. Davis, E. Carcole, and D. M. Cottrell, "Nondiffracting interference patterns generated with programmable spatial light modulators," Applied Optics **35**, 599–602 (1996).
21. A. Hakola, T. Hakkarainen, R. Tommila, and T. Kajava, "Energetic Bessel–Gauss pulses from diode-pumped solid-state lasers," JOSA B **27**, 2342–2349 (2010).
22. A. N. Khilo, E. G. Katranji, and A. A. Ryzhevich, "Axicon-based Bessel resonator: analytical description and experiment," JOSA A **18**, 1986–1992 (2001).
23. C. Paterson and R. Smith, "Higher-order Bessel waves produced by axicon-type computer-generated holograms," Optics Communications **124**, 121–130 (1996).
24. S. H. Tao, X. C. Yuan, and B. S. Ahluwalia, "The generation of an array of nondiffracting beams by a single composite computer generated hologram," Journal of Optics A: Pure and Applied Optics **7**, 40–46 (2005).
25. V. Arrizón, U. Ruiz, D. Aguirre-Olivas, D. Sánchez-de-la Llave, and A. S. Ostrovsky, "Comparing efficiency and accuracy of the kinoform and the helical axicon as Bessel-Gauss beam generators." JOSA A **31**, 487–492 (2014).
26. L. C. Andrews, R. L. Phillips, R. Crabbs, D. Wayne, T. Leclerc, and P. Sauer, "Atmospheric channel characterization for orca testing at nttr," in "LASE," , O. Korotkova, ed. (SPIE, 2010), pp. 758809–758809–12.
27. R. G. Lane, A. Glindemann, and J. C. Dainty, "Simulation of a Kolmogorov phase screen," Waves in Random Media **2**, 209–224 (1992).
28. J. D. Schmidt, *Numerical Simulation of Optical Wave Propagation with Examples in MATLAB* (SPIE, Bellingham, Washington, 2010).